

Exploring Text-Guided Single Image Editing for Remote Sensing Images

Fangzhou Han, Lingyu Si, Hongwei Dong, *Member, IEEE*, Lamei Zhang, *Senior Member, IEEE*,
Hao Chen, *Member, IEEE* and Bo Du, *Senior Member, IEEE*

arXiv:2405.05769v2 [cs.CV] 26 Sep 2024

Abstract—Artificial intelligence generative content (AIGC) has significantly impacted image generation in the field of remote sensing. However, the equally important area of remote sensing image (RSI) editing has not received sufficient attention. Deep learning based editing methods generally involve two sequential stages: generation and editing. During the generation stage, consistency in content and details between the original and edited images must be maintained, while in the editing stage, controllability and accuracy of the edits should be ensured. For natural images, these challenges can be tackled by training generative backbones on large-scale benchmark datasets and using text guidance based on vision-language models (VLMs). However, these previously effective approaches become less viable for RSIs due to two reasons: First, existing generative RSI benchmark datasets do not fully capture the diversity of remote sensing scenarios, particularly in terms of variations in sensors, object types, and resolutions. Consequently, the generalization capacity of the trained backbone model is often inadequate for universal editing tasks on RSIs. Second, the large spatial resolution of RSIs exacerbates the problem in VLMs where a single text semantic corresponds to multiple image semantics, leading to the introduction of incorrect semantics when using text to guide RSI editing. To solve above problems, this paper proposes a text-guided RSI editing method that is controllable but stable, and can be trained using only a single image. It adopts a multi-scale training approach to preserve consistency without the need for training on extensive benchmark datasets, while leveraging RSI pre-trained VLMs and prompt ensembling (PE) to ensure accuracy and controllability in the text-guided editing process. High-quality RSI editing results can be achieved by first applying multi-scale training to the target image, followed by text-guided fine-tuning using RSI pre-trained VLMs and PE. Experimental results on multiple RSI editing tasks show that the proposed method offers significant advantages in both CLIP scores and subjective evaluations compared to existing methods. Additionally, we explore the ability of the edited RSIs to support disaster assessment tasks in order to validate their practicality. Codes will be released at https://github.com/HIT-PhilipHan/remote_sensing_image_editing.

Index Terms—Remote sensing image editing, single image diffusion, image generation, text-guided image editing, prompt ensembling.

This work was supported in part by the National Natural Science Foundation of China under Grant 62271172, Grant 62301539 (*Corresponding author: Hongwei Dong*).

F. Han, H. Dong, L. Zhang and H. Chen are with the Department of Information Engineering, Harbin Institute of Technology, Harbin, China (e-mail: donghongwei1994@163.com, {lmzhang, hit_hao}@hit.edu.cn).

L. Si is with the National Key Laboratory of Space Integrated Information System, Institute of Software, Chinese Academy of Sciences, Beijing, China (e-mail: lingyu@iscas.ac.cn).

B. Du is with the Hubei Luojia Laboratory, National Engineering Research Center for Multimedia Software, School of Computer Science, Wuhan University, Wuhan, China (e-mail: dubo@whu.edu.cn).

F. Han and L. Si contributed equally to this paper.

I. INTRODUCTION

BECAUSE of the extensive coverage and wealth of information, remote sensing images (RSIs) have facilitated various vital tasks such as disaster response, environmental monitoring, and urban planning [1], [2]. Nowadays, the cost of remote sensing has significantly decreased, providing sufficient data for long-term observations of stable areas such as farmland, mountains and cities. However, in extreme events such as earthquakes, forest fires, and tsunamis, timely and comprehensive observation is challenging due to their low frequency of occurrence and high randomness in location. The difficulty in obtaining RSIs for such scenarios further hinders their prevention, detection, and assessment.

It is important to note the strong correlation between extreme and conventional scenarios, where the basic semantic of objects in RSIs remain unchanged, but new semantic information is added, such as transforming a tree into a burning tree. This allows for the acquisition of a large number of RSIs for extreme scenarios by editing RSIs from conventional ones. However, the significant importance of RSI editing has largely been overlooked in current research.

While research on image editing remains insufficient, the field of remote sensing has already seen comprehensive studies on image generation, which serves as both the foundation and the initial stage of editing. In recent years, the development of deep learning has led to extensive applications of generation networks, such as variational autoencoder (VAE) [3] and generative adversarial network (GAN) [4], [5]. These advancements have led to significant breakthroughs in remote sensing field, including sample augmentation [6]–[8], image super-resolution [9]–[11], cross-modal image transformation [12]–[14], and cloud removal [15], [16]. VAE generates images by sampling from the latent distribution mapped from the training images, while GAN produces sufficiently realistic image generation results through adversarial games between the generator and discriminator. Although the aforementioned methods perform well in generation tasks, their aim is to fit the distribution of existing data and do not have the ability to introduce new semantics required for editing. More importantly, the development of remote sensing platforms has significantly reduced the cost of obtaining RSIs in conventional scenarios, greatly diminishing the need for unconditional generation of RSIs.

Unlike image generation, the core of image editing lies in introducing new semantic information into the target image, which requires guidance from additional information.

This is inherently a challenging task, but the emergence of vision-language models (VLMs) offers an excellent approach for providing this additional information [17]. For instance, the seminal work in VLMs, contrastive language-image pre-training (CLIP), achieves semantic alignment between text and images through pre-training on large-scale paired text-image datasets [18], which is essential for text-guided image editing. Subsequently, the integration of CLIP with various generative models, such as GANs and denoising diffusion probabilistic models (DDPMs) [19] has led to significant advancements in controllable text-guided image editing [20], [21]. Generally, such methods can be classified into below categories [22]: training-based approaches [23], [24], testing-time fine-tuning approaches [25], [26], training and fine-tuning free approaches [27], [28]. Training-based methods are distinguished not only by their robust training of diffusion models and their effective data distribution modeling, but also by their reliable performance across diverse editing tasks. In contrast, testing-time fine-tuning approaches offer greater precision and controllability, while fine-tuning free methods are significantly faster and more cost-efficient. While these methods have led to significant advancements in image editing performance, applying these existing models to the field of remote sensing presents numerous challenges. Specifically, deep learning based image editing models can be progressively divided into two stages: generation and editing. In the generation stage, the model produces content that maintains semantic consistency with the original image, while in the editing stage, new semantic information is introduced to fulfill the editing objectives. Next, we will analyze the potential factors within each of these two stages that contribute to the poor performance of conventional editing models on RSIs.

Firstly, during the generation stage, conventional image editing models struggle to preserve content and specific details from the original RSIs, such as background elements and the identity of objects within them [29]. This limitation arises because the models, when applied to natural images, rely on DDPMs trained on large and diverse benchmark datasets, which equips them to generate images across a broad spectrum of complex scenarios. However, for RSIs, the above approach no longer works because remarkable domain discrepancies often arise in terms of resolution, perspective, and other sensor-related factors between the images used for training and those intended for editing [30]. Furthermore, the semantic information pertinent to the RSIs requiring edited may be underrepresented in the training dataset, such as uncommon ships, buildings, and newly emerged land cover types [31], [32]. As a result, backbones trained on RSI benchmark datasets lack sufficient generalization capability required to effectively handle the diverse editing tasks needed for RSIs.

Secondly, during the editing stage, conventional text-guided image editing models face the challenge of semantic mismatches between text and images. This issue arises from two key reasons. First, VLMs used in conventional editing methods are typically pre-trained on natural text-image pairs, limiting their capacity to effectively interpret RSIs. Second, RSIs have a much higher spatial coverage compared to natural images, often containing multiple semantic elements [33]. However,

pre-trained VLMs like CLIP typically align the entire image with a single text description, and this one-to-many correspondence leads to inaccurate semantic alignment. Fig. 1 illustrates the aforementioned problem with an example. Such semantic mismatches can easily result in inaccurate outcomes from the model during the text-guided editing process.

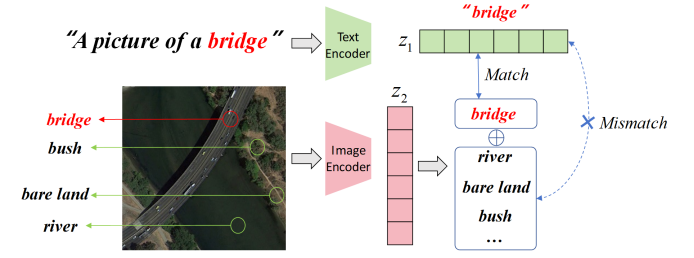


Fig. 1. Semantic mismatches between text and images. In the image, semantic information encompasses not just the bridge but also the river, bush, bare land, and other surrounding elements. However, the corresponding textual semantic information often refers to the most prominent part of the image, which in this case is the bridge.

To tackle the aforementioned challenges, this paper proposes a text-guided image editing method customized for RSIs, with optimizations applied concurrently in both the image generation and editing stages of the RSI editing process. To address the issue of semantic inconsistency before and after editing, we implement a multi-scale training strategy using only the target image for DDPM training, which essentially eliminates the semantic inconsistency in the generation process caused by domain discrepancies. To address the issue of text-image semantic mismatch in the editing stage, we leverage a RSI pre-trained CLIP model to incorporate remote sensing information into image editing. Additionally, we introduce prompt ensembling (PE), which generates similar text through large language models (LLMs). Combining multiple texts helps align text embeddings more closely with the desired image embeddings and avoids introducing anomalous semantics. Overall, the contributions of this paper are as follows:

- 1) We focus on the relatively overlooked but important issue of RSI editing and propose a RSI-customized method that achieves stable and controllable text-guided RSI editing.
- 2) We implement a multi-scale training strategy with a single image to solve the problem of lacking corresponding RSIs for editing tasks, thereby maintaining consistency in content and details between the original and edited images.
- 3) We leverage RSI pre-trained CLIP and propose the PE technique to address the issue of irrelevant semantic interference during editing, ensuring the accuracy of text-guided editing results.
- 4) Extensive experimental results demonstrate that the proposed method is adaptable to various RSI editing tasks.

II. RELATED WORKS

A. Generation Models in Remote Sensing Field

In recent years, with the advancement of deep generative models, RSIs generation has yielded significant results

in various tasks, including data augmentation, image super-resolution, cross-modal image transformation, and cloud removal. Broadly speaking, the generative models predominantly used in the field of remote sensing are GANs and DDPMs.

As to the GANs, for the data augmentation task, Zhang *et al.* [34] proposed a data augmentation method based on variational autoencoder multi-scale GAN with spatial and channel wise attention to balance the sample distribution and improve the subsequent ROI extraction results. Chen *et al.* [35] proposed a novel data-level solution, namely, instance-level change augmentation, to generate bitemporal images that contain changes involving plenty and diverse buildings by leveraging generative adversarial training. Then, they proposed context-aware blending for a realistic composite of the building and the background. For the image super-resolution task, Dong *et al.* [36] explored the potential of the reference-based super-resolution method on RSIs, utilizing rich texture information from high resolution reference images to reconstruct the details in low resolution images. Song *et al.* [37] proposed a new multilevel feature fusion with GAN for generating fusion remote sensing satellite images with both high-temporal and high-spatial resolution. For the cross-modal image transformation task, Yang *et al.* [38] proposed a fine-grained GAN on SAR-to-optical image translation, introducing novel strategies such as unbalanced generator, multi-scale discriminator and comprehensive normalization group to enhance the detailed information in generated optical images.

Recently, DDPM-based models have also gained traction in the field of remote sensing image generation, particularly in super-resolution tasks. For instance, Xiao *et al.* [39] introduced a DDPM-based approach for RSI super-resolution called EDiffSR. EDiffSR was not only easy to train but also retained the advantages of DDPM in generating perceptually pleasing images. Experiments on remote sensing datasets demonstrated that EDiffSR could effectively restore visually appealing images in both simulated and real-world RSIs. Additionally, Zhang *et al.* [40] proposed a diffusion-based super-resolution method named texture consistency diffusion model for large-factor RSIs, which framed the large-factor super-resolution task as a reference-guided diffusion process and explored how to integrate pixel-wise constraints into the diffusion model.

B. Denoising Diffusion Probabilistic Model (DDPM)

In the process of diffusion, DDPMs convert the original data into a normal distribution, which means that every point on the normal distribution is a map of the real data, thus enhancing the interpretability of the model. Meanwhile, compared with GANs, the diffusion model mitigates the problems such as collapse during training, and the quality of images generated is improved. In recent years, research on the structure, optimization goals and application scenarios of DDPM model has become increasingly abundant. For example, as to the model structure and the optimization goals, Peebles *et al.* [41] explored a new class of diffusion models based on the transformer architecture. The model trained latent diffusion models of images, replacing the commonly used U-Net backbone with a transformer that operates on latent patches.

Kingma *et al.* [42] introduced a family of diffusion-based generative models that obtain state-of-the-art likelihoods on standard image density estimation benchmarks. It showed that the variational lower bound simplifies to a remarkably short expression in terms of the signal-to-noise ratio of the diffused data, improving the theoretical understanding of this model class. In addition, not only in the nature image generation task, Ho *et al.* [43] made progress by proposing a diffusion model for video generation that shows very promising initial results. Wu *et al.* [44] proposed MedSegDiff, the first DPM-based model for general medical image segmentation tasks. To enhance the step-wise regional attention in DDPM for medical image segmentation, MedSegDiff proposed dynamic conditional encoding, which established state-adaptive conditions for each sampling step. Additionally, MedSegDiff proposed the feature frequency parser to eliminate the negative effect of high-frequency noise components in this process. And DDPMs can also be used for tasks such as image compression. For example, Yang *et al.* [45] outlined an end-to-end optimized lossy image compression framework using diffusion generative models. The approach relied on the transform coding paradigm, where an image was mapped into a latent space for entropy coding and, from there, mapped back to the data space for reconstruction.

C. Image Editing Methods

In the field of AIGC, which utilizes artificial intelligence to create and modify digital content, image editing is considered an important area for innovation and practical applications. Generally, such image editing methods can be classified into below categories [22]: training-based approaches, testing-time fine-tuning approaches, training and fine-tuning free approaches.

As to the training-based approaches, Kawar *et al.* [29] demonstrated, for the very first time, the ability to apply complex (e.g., non-rigid) text-based semantic edits to a single real image. The method, called Imagic, leveraged a pre-trained text-to-image diffusion model for this task. It produced a text embedding that aligned with both the input image and the target text, while fine-tuning the diffusion model to capture the image-specific appearance. Moreover, Kwon *et al.* [46] proposed asymmetric reverse process which discovers the semantic latent space in frozen trained diffusion models. The semantic latent space, named h-space, has nice properties for accommodating semantic image manipulation: homogeneity, linearity, robustness, and consistency across time-steps.

For the testing-time fine-tuning approaches, these approaches range from fine-tuning the entire denoising model to focusing on specific layers or embeddings. For example, Mokady *et al.* [25] introduced an accurate inversion technique and thus facilitate an intuitive text-based modification of the image. They only modify the unconditional textual embedding that is used for classifier-free guidance, rather than the input text embedding. To better align with specific editing intentions. Zhang *et al.* [26] perceived style as a learnable textual description of a painting and propose an inversion-based style transfer method, which can efficiently and accurately learned the key

information of an image, thus capturing and transferring the artistic style of a painting.

Finally, for the training and fine-tuning free approaches, they are fast and low-cost because they do not require any form of training (on the dataset) or fine-tuning (on the source image) during the complete process of editing. For example, Wallace *et al.* [27] proposed Exact Diffusion Inversion via Coupled Transformations (EDICT), an inversion method that drawn inspiration from affine coupling layers. EDICT enabled mathematically exact inversion of real and model-generated images by maintaining two coupled noise vectors which were used to invert each other in an alternating fashion. Pan *et al.* [47] tried to predict multiple noises during single-step sampling to solve the problem of reconstruction failure. By using a novel blended guidance technique, they show that effective results could be obtained on a large range of image editing tasks without large classifier-free guidance in inversion.

Although diffusion-based image editing models have garnered widespread attention in fields such as medical image processing and computer vision, their potential remains underexplored in the domain of remote sensing.

III. METHODOLOGY

A. Multi-scale training strategy based on single image

The training process of conventional DDPMs typically requires a large number of samples to ensure the effective generation of images from noise. Although extensive benchmark datasets provide DDPMs with generative capabilities, remote sensing images exhibit significant variations in resolution, color, and other factors across different sensors. This results in inadequate generalization for backbones trained on such datasets, causing semantic inconsistencies between the original and edited RSIs. To resolve this, we introduce a multi-scale DDPM training strategy, termed SinDDM, which operates with a single image, maintaining consistency in content and details between the original and edited RSIs.

We describe SinDDM by starting with the conventional DDPM training process. The idea behind DDPM is to define a Markov chain with diffusion steps to incrementally introduce random noise to the data, and subsequently learning to reverse this diffusion process to reconstruct the desired image from the noise. Therefore, the DDPM can be divided into two process: forward process and backward process. The structure comparison of DDPM, VAEs and GANs is shown in the Fig. 2. SinDDM is consistent with the conventional DDPM in the construction of denoising model while the difference is that SinDDM constructs multi-scale pyramid by down-sampling the input single image in the training process, and trains the denoising model since the smallest scale. Upon completion of denoising at a specific scale, the process transitions to denoising at the subsequent scale through up-sampling. Therefore, in the original DDPM, there is only one parameter T , representing the number of noise addition steps in the forward process, while in the SinDDM, a new parameter S is added to denote the scale within the denoising model. The whole multi-scale diffusion is shown in Fig. 3.

First, we could construct the image pyramid $\{x^{N-1}, x^{N-2}, \dots, x^0\}$ while every image x^s of the pyramid

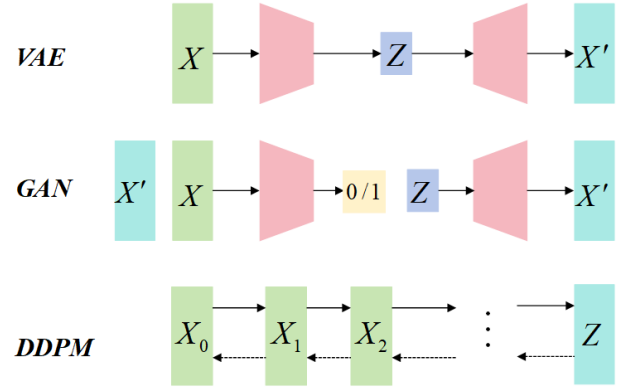


Fig. 2. The structure comparison of the VAE, GAN and the DDPM.

is generated via the down-sampling factor r . We use bicubic interpolation for both the upsampling and downsampling operations. Then, for one scale $s \in (0, 1, \dots, N-1)$, the forward process $q(x_t^s | x_{t-1}^s)$ could be expressed by the following formula:

$$q(x_t^s | x_{t-1}^s) = \mathcal{N}(x_t^s; \sqrt{1 - \beta_t} x_{t-1}^s, \beta_t I) \quad (1)$$

where the t represents the steps of forward process to add noise to the image, which grows from 0 to T and the β_t is the variance taken at each step, which is between 0 and 1. we use α_t to replace $1 - \beta_t$ and DDPM uses a linear variance schedule, modeling the denoising process a Markov chain:

$$q(x_{1:T}^s | x) = \prod_{t=1}^T q(x_t^s | x^s). \quad (2)$$

Then through reparameterization trick, the noise image x_t^s of any step can be sampled directly based on the original data x^s :

$$\bar{\alpha}_t = \prod_{i=1}^t \bar{\alpha}_i \quad (3)$$

$$x_t^s = \sqrt{\bar{\alpha}_t} x^s + \sqrt{1 - \bar{\alpha}_t} \epsilon, \quad \text{while } \epsilon \sim \mathcal{N}(\mathbf{0}, \mathbf{I})$$

where, the ϵ is the noise. When step grows, the $\bar{\alpha}_t$ decreases monotonically from 1 to 0, which ensures that the resulting image x_T is close to random noise.

It should be noted that due to the upsampling and downampling operations based on interpolation, the generated image will be blurred, so it is necessary to achieve de-blurring while de-noising in the training process. To do this, we blend the noisy image with its blurry version. We construct a blurry version of the pyramid $\{x^{N-1}, x^{N-2}, \dots, x^0\}$, which could be represented as $\{\tilde{x}^{N-1}, \tilde{x}^{N-2}, \dots, \tilde{x}^0\}$, where $\tilde{x}^0 = x^0$ and $\tilde{x}^s = (x^{s-1})^{\uparrow r}$. Then, by combining the noise and the blurred version linearly, we could get the multi-scale diffusion process over (s, t) :

$$x_t^s = \sqrt{\bar{\alpha}_t} [\gamma_t^s \tilde{x}^s + (1 - \gamma_t^s) x^s] + \sqrt{1 - \bar{\alpha}_t} \epsilon \quad (4)$$

where the γ_t^s is the mixing coefficient, which increases monotonically from 0 to 1.

In the training process, a single fully convolutional model is trained to predict x_0^s from the x_T^s . Because the noisy image

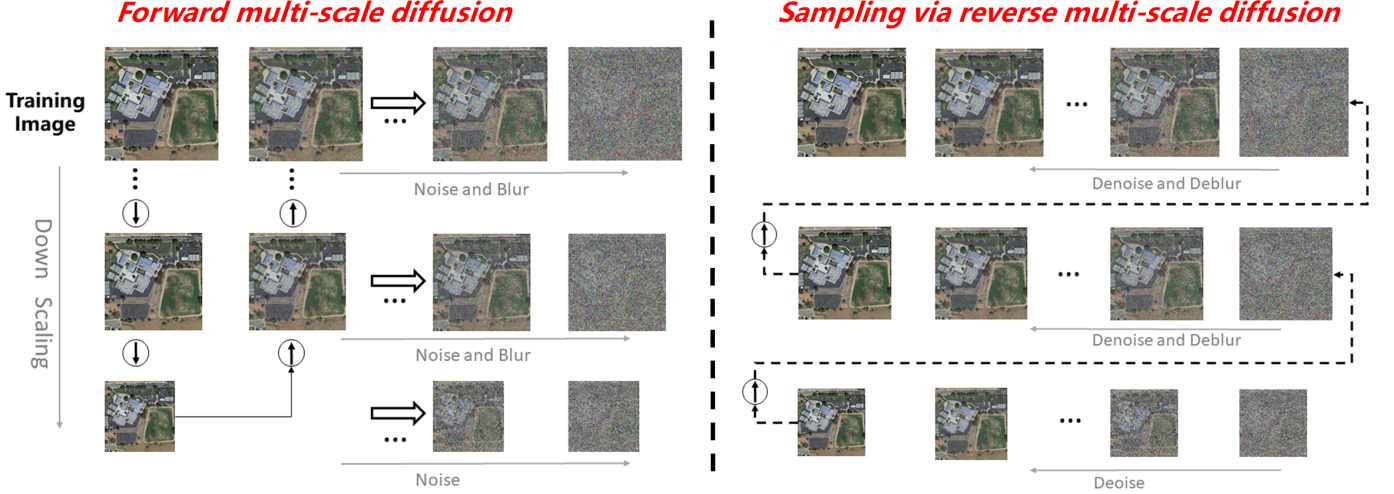


Fig. 3. The multi-scale training strategy. The forward multi-scale diffusion process (left) construct a sequence of images that are linear combinations of the original images in multi scale, their blurry version, and noise. For the sampling process via reverse multi-scale diffusion (right) starts from pure noise at the coarsest scale. In each scale, SinDDM gradually removes the noise until reaching a clean image, which is then upsampled and combined with noise to start the process again in the next scale. It is worth noting that the above process uses a multi-scale training strategy, so just a single image could achieve effective training of DDPM.

Algorithm 1 Training Procedure of SinDDM

```

1: repeat
2:    $x^s \sim q(x^s)$ 
3:    $t \sim \text{Uniform}(\{1, \dots, T\})$ 
4:    $s \sim \text{Uniform}(\{1, \dots, N\})$ 
5:    $\epsilon \sim \mathcal{N}(\mathbf{0}, I)$ 
6:   Update model  $\epsilon_\theta$  by taking gradient descent step on:
7:    $\nabla_\theta \|\epsilon - \epsilon_\theta(\sqrt{\bar{\alpha}_t}[\gamma_t^s \tilde{x}^s + (1 - \gamma_t^s)x^s] + \sqrt{1 - \bar{\alpha}_t}\epsilon)\|^2$ 
8: until converged

```

is generated by adding the fixed noise according to the noise schedule, which is known, the goal of SinDDM is to gradually predict the noise ϵ added in the forward phase. First, we can model the recursive process of Markov chain in the single step of the diffusion process:

$$p_\theta(x_{t-1}^s | x_t^s) = \mathcal{N}(x_{t-1}^s; \mu_\theta^s(x_t^s, t), \beta_t^s I) \quad (5)$$

where the $\mu_\theta(x_t^s, t)$ could be calculated as follows:

$$\mu_\theta(x_t^s, t) = \frac{1}{\sqrt{\alpha_t}}(x_t^s - \frac{1 - \alpha_t}{\sqrt{1 - \bar{\alpha}_t}}\epsilon(x_t^s, t)). \quad (6)$$

In the optimization process, the KL divergence is optimized to make the predicted distribution $p_\theta(x_{t-1}^s | x_t^s)$ closer to the real distribution $q_\theta(x_{t-1}^s | x_t^s, x_0^s)$. Thus, the optimization objective θ can be translated into calculating the Kullback-Leibler divergence D_{KL} of the above two distributions:

$$\theta = \arg \min_{\theta} D_{KL}(q_\theta(x_{t-1}^s | x_t^s, x_0^s) \| p_\theta(x_{t-1}^s | x_t^s)). \quad (7)$$

Since the above distributions have the same variance, the Kullback-Leibler divergence can be simplified:

$$D_{KL} = \frac{1}{2} \sum_t \|\mu_t(x_t^s, x_0^s) - \mu_\theta(x_t^s, t)\|^2 + C \quad (8)$$

where the C is a constant and the \sum_t is the covariance matrix of multivariate Gaussian distribution. However, it is difficult

to directly make the model predict μ_θ , because the distribution of the μ_θ is relatively uncertain and has a wide range of values, so the above prediction of the mean can be converted into a prediction of ϵ_θ . Then, through reparameterization techniques [19], the following simple loss function can be obtained:

$$L_{t-1}^s = \mathbb{E}_{x_t^s, \epsilon} [\|\epsilon - \epsilon_\theta(\sqrt{\bar{\alpha}_t}x_t^s + \sqrt{1 - \bar{\alpha}_t}\epsilon, t, s)\|_1] \quad (9)$$

where the ϵ_θ is prediction of the fully convolutional model. The overall training procedure is shown in Algorithm 1.

As to the diffusion process, the sampling via the reverse multi-scale diffusion starts from pure noise at the coarsest scale. In each scale, the SinDDM gradually removes the noise until reaching a clean image, which is then upsampled and combined with noise to start the process again in the next scale. The process will repeat until the scale $s = 0$ comes to $s = N - 1$. When $s = 0$, we follow the standard approach, which starts with random noise at $t = T$ and gradually removing noise until a clean sample is obtained at $t = 0$. When $s > 0$, we use σ except when applying text-guidance in which case we also use the DDPM scheduler. As shown in Algorithm 2, the proposed model is conditioned on both the time step t and the scale s , which is proved to improve generation quality and training time compared to a separate diffusion model for each scale.

As shown in Fig. 4, we use a fully-convolutional model with four blocks to achieve the process of noise prediction. As opposed to conventional DDPMs, the proposed model uses only convolutions and GeLU nonlinearities, without any self-attention or downsampling/upsampling operations. At the same time, we use the time step t and scale s as the condition to train the DDPM. Similar to the conventional DDPMs, which only embed time t as a condition, we infuse the t and s to the model using a joint embedding. The time-step t and scale s first pass through an embedding block, in which they go through sinusoidal positional embedding (SPE) and then be

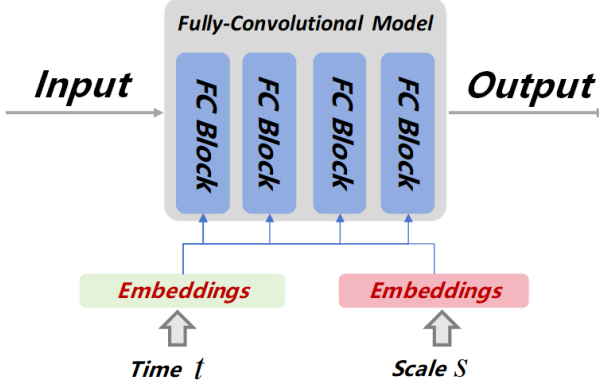


Fig. 4. The architecture of the proposed DDPM model. The fully-convolutional model is based on four blocks and uses the time step t and scale s as the condition to train.

concatenated and passed through two fully-connected layers with GeLU activation to yield a time-scale embedding vector ts . The SPE is derived from transformer model [48], which is a technique in which the position of each element in a sequence is embedded into a model. The main idea is to assign a unique code to each location by mapping each location to a fixed sinusoidal function in a high-dimensional space. Taking the SPE of t as an example, the calculation formula is as follows:

$$\begin{aligned} SPE(t, 2i) &= \sin(t/10000^{2i/d}) \\ SPE(t, 2i + 1) &= \cos(t/10000^{2i/d}) \end{aligned} \quad (10)$$

where the d is the embedding dimension of the s after SPE and the i represents the number of the dimension. Similarly, the scale parameter s can also be obtained by the SPE and has the same size as the code value of t . The embedding procedure is shown in the Fig. 5.

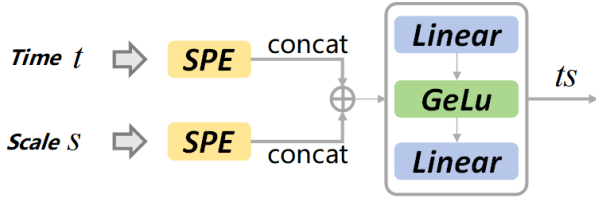


Fig. 5. The architecture of the embedding model of the time-step t and scale s .

As for the fully-convolutional blocks, as shown in Fig. 6, the pipeline consists of 2D convolutions with a residual connection and GeLU function, and the input time-scale embedding ts vector is passed through a GeLU activation and a fully-connected layer. In each training iteration we sample a batch of noisy images from the same randomly chosen scale s but from several randomly chosen time steps t . We used the Adam optimizer to train 12,000 epochs during the training procedure.

B. The Prompt-guided Fine-tuning Process

The core objective of image editing is to incorporate new semantic information, typically in the form of ROIs or text, known as prompts. Various methods exist for embedding

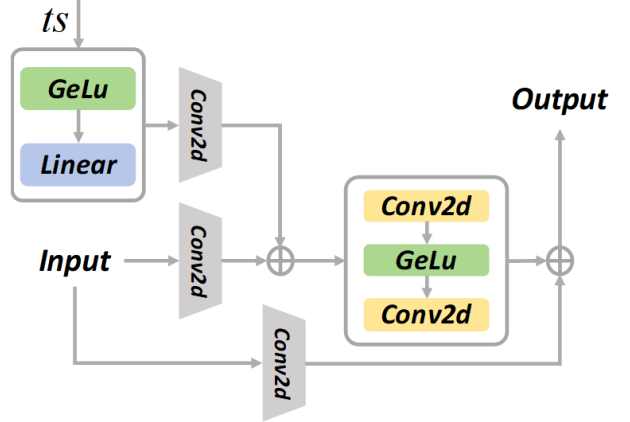


Fig. 6. The architecture of the block.

Algorithm 2 Sampling Procedure of SinDDM

```

1: for  $s = 0, 1, 2, \dots, N - 1$  do
2:   if  $s = 0$  then
3:      $x_{T[0]}^0 \sim \mathcal{N}(\mathbf{0}, \mathbf{I})$ 
4:   end if
5:   for  $t = T[s], T[s - 1], \dots, 0$  do
6:      $x_t^{s, mix} = \frac{x_t^s - \sqrt{1 - \bar{\alpha}_t} \epsilon_\theta(x_t^s, t, s)}{\sqrt{\bar{\alpha}_t}}$ 
7:      $\hat{x}_0^s = \frac{x_t^{s, mix} - \gamma_t^s \hat{x}^s}{1 - \gamma_t^s}$ 
8:      $x_{t-1}^{s, mix} = \gamma_{t-1}^s \hat{x}^s + (1 - \gamma_{t-1}^s) \hat{x}_0^s$ 
9:      $\mathbf{z} \sim \mathcal{N}(\mathbf{0}, \mathbf{I})$ 
10:     $x_{t-1}^s = \sqrt{\bar{\alpha}_t} \hat{x}_{t-1}^{s, mix} + \sqrt{1 - \bar{\alpha}_{t-1} - (\sigma_t^s)^2} \frac{x_{t-1}^{s, mix} - \sqrt{\bar{\alpha}_t} x_t^{s, mix}}{\sqrt{1 - \bar{\alpha}_t}} + \sigma_t^s \mathbf{z}$ 
11:  end for
12:  if  $s < N - 1$  then
13:     $\hat{x}^{s+1} = \hat{x}_0^s \uparrow^r$ 
14:     $\mathbf{z} \sim \mathcal{N}(\mathbf{0}, \mathbf{I})$ 
15:     $x_{T[s+1]}^{s+1} = \sqrt{\bar{\alpha}_{T[s+1]}} \hat{x}^{s+1} + \sqrt{1 - \bar{\alpha}_{T[s+1]}} \mathbf{z}$ 
16:  end if
17: end for
18: end for

```

semantic information from prompts into DDPMs [22]. In our proposed approach, we leverage CLIP to extract text embeddings from the prompts and apply CLIP loss as supervision to fine-tune the sampling process of SinDDM, as depicted in Fig. 7.

Specifically, the trained SinDDM is fine-tuned using different types of prompt guidance. The ROI prompt is used to mask regions of the original image that do not require modification, while text prompts are refined with PE. Given its alignment across hundreds of millions of image-text pairs, CLIP contains rich multi-modal representational information, making it an optimal choice for incorporating text-based semantic information.

To use CLIP as the guidance, first, the current generated image \hat{x}_0^s and the text prompts provided by the users are sent to the image encoder $f_I(\cdot)$ and text encoder $f_T(\cdot)$ of the CLIP model, respectively. Then, we use the cosine similarity loss function to measure the discrepancy between the above two embeddings and regard it as an optimization target in the

process of fine-tuning. Therefore, the CLIP loss L_{CLIP} can be depicted as follows:

$$L_{CLIP} = -\frac{f_I(\hat{x}_0^s) \cdot f_T(\text{text})}{|f_I(\hat{x}_0^s)| \cdot |f_T(\text{text})|}. \quad (11)$$

The prompts provided by the users can be divided into two types: when they are only text prompts, the above CLIP-guidance stops at $s = N - 1$ to produce a smoother edited image. However, if the prompts include both the ROI limiting the editing area and the corresponding text, the affected regions would be constrained the spatial extent by zeroing out all gradients outside the ROI mask. This mask is calculated in the first step CLIP is applied, and is kept fixed for all remaining time steps and scales (it is upsampled when going up the scales of the pyramid). We define the mask generated by ROI as m^s , then during the fine tuning procedure, we could update the \hat{x}_0^s via the following formula:

$$\hat{x}_0^s \leftarrow \eta \delta m^s \odot \nabla L_{CLIP} + (1 - m^s) \odot \hat{x}_0^s \quad (12)$$

where the $\eta \in [0, 1]$ is an strength parameter that controls the intensity of the CLIP guidance and the $\delta = \|\hat{x}_0^s \odot m^s\| / \|\nabla L_{CLIP} \odot m^s\|$. Due to the strong prior of the proposed denoiser, which is overfitted to the statistics of the training image, the simple update steps tend to be ineffective. In order to avoid the resolution of the original CLIP gradient at each denoiser step, the update rule of \hat{x}_0^s will be transformed like follows with a momentum:

$$\hat{x}_0^s \leftarrow \eta \delta m^s \odot \nabla L_{CLIP} + (1 - m^s) \odot (\lambda \hat{x}_0^s + (1 - \lambda) \hat{x}_{0,prev}^s) \quad (13)$$

where the $\hat{x}_{0,prev}^s$ is the \hat{x}_0^s from the previous time-step and the η is a momentum parameter which is set to 0.05.

Meanwhile, the original image x_0^s is added with the same noise and blended with the masked image to continue the diffusion process, which will improve the smooth transition between the edge of the edited content in the ROI region and the original image. It is worth noting that, since the CLIP model's image and text encoder is only used to generate the embeddings during the fine-tuning process, their parameters are also frozen and do not participate in back propagation.

Since in image editing, in addition to using text as guidance, the original region prompt in the image is also crucial, especially when the texts could not accurately describe the edited target. At this point, our proposed method use ROI to choose a specific area of the image and copy the content of the specific area at the specified location to achieve ROI-prompted image editing. In this way, the user can choose to replicate the targets to a specific area, which is very useful for some repetitive targets, such as tightly packed vehicles, oil storage tanks laid out in port terminals, and wind turbines and photovoltaic panels arranged on various scenes. To be more specific, we use x_{target}^s to be an image containing the desired contents within the target ROIs, while the m^s be a binary mask indicating the ROIs, both down-sampled to scale s . Then we use an simple L^2 loss to achieve the ROI guidance:

$$L_{ROI} = \|m^s \odot (\hat{x}_0^s - \hat{x}_{t \arg et}^s)\|^2. \quad (14)$$

In the sampling procedure, we update the \hat{x}_0^s by taking a gradient step on this loss, while mix \hat{x}_{target}^s and \hat{x}_0^s with the step size η . Namely:

$$\begin{aligned} \hat{x}_0^s \leftarrow m^s \odot ((1 - \eta) \hat{x}_0^s + \eta \cdot x_{target}^s) \\ + (1 - m^s) \odot \hat{x}_0^s \end{aligned} \quad (15)$$

where the η determines the strength of the effect. We use this guidance in all scales except for the finest one.

C. Prompt Ensembling

Recently, prompt based fine-tuning is widely used in the application of multiple foundation models [49]–[51]. Unlike conventional fine-tuning approaches, the prompt-based paradigm harmoniously unifies the trained DDPMs and downstream tasks within the same framework. Thus, choosing the right prompt is critical to the effectiveness of downstream tasks. For the text-guided image editing method, the text prompts provided by the users have a great influence on the result of image editing, especially if the CLIP itself is potentially biased. For example, when the user uses “Large Fire” as text prompt to generate an image depicting a ship on fire, since “Fire” is often associated with grassland in the semantic information of CLIP, the edited image area will have an unreasonable result of grass on board. Nevertheless, when the user used “heavily burning” as the prompt, the results will much closer to the authentic situations. Fig. 8 depicts the influence of the different text prompts.

The reason for the aforementioned unsatisfactory generation results lies in the fact that, within CLIP, text semantics and image semantics exhibit a one-to-many correspondence. This makes it challenging to find an ideal image embedding using a single text embedding. Recent studies have demonstrated that employing multiple prompts can further enhance the performance of prompt learning, a technique known as multi-prompt learning. Among the most straightforward and effective approaches, PE mitigates the generation of irrelevant content by combining multiple text prompts with the same semantics expressed in different forms. Consequently, we employ PE in our proposed method as a pre-processing strategy to produce robust text guidance. Additionally, for diversity, we leverage ChatGPT as a generation tool to quickly produce high-quality prompts. The overall structure is illustrated in Fig.9.

Utilizing LLMs such as ChatGPT, the original text is leveraged to generate various semantically similar text prompts. These augmented text prompts enhance the information provided by the user and transform it into multiple forms. For instance, when the user's input is “A ship is on fire,” we use the following command to instruct ChatGPT to generate corresponding augmented text prompts:

“I need you act as a text prompt generator. I will give you a text prompt that you need to use common sense to translate into a total of five prompts with different descriptions but similar meanings. Each prompt given meets the same syntax format as the original text prompt and is concise and easy to understand. Here is an example: Given “A ship is on fire”, you need to take into account the actual scenario of the ship on fire and generate the approximate description “A ship is

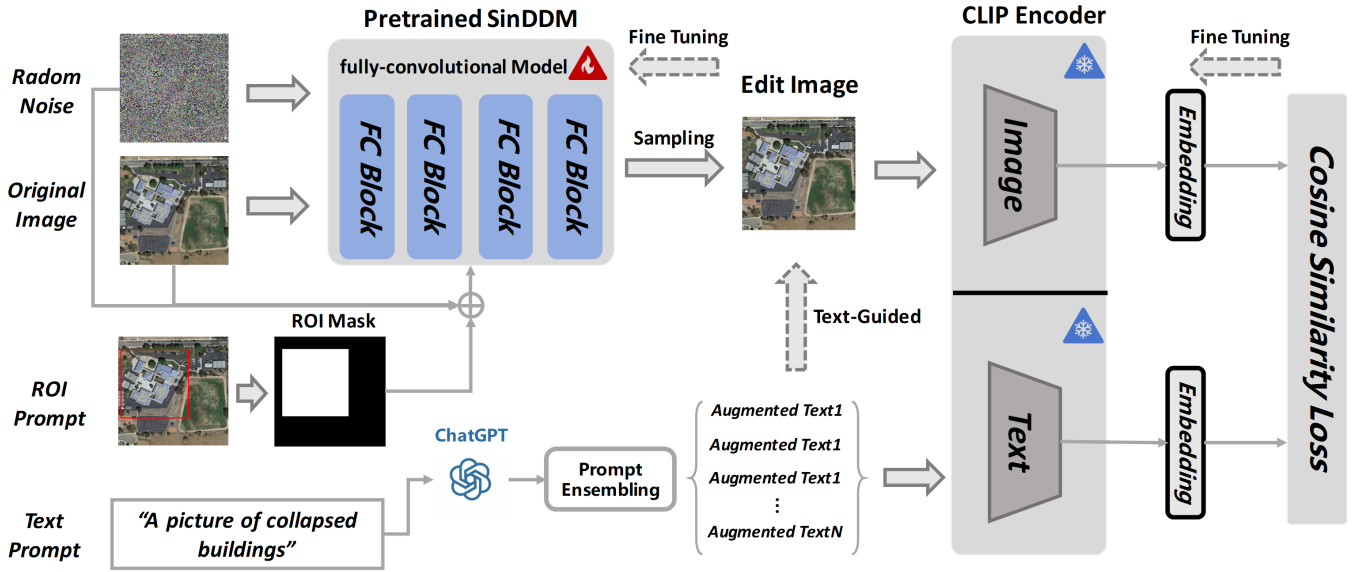


Fig. 7. The prompt-guided fine-tuning process of SinDDM. After the training procedure, the encoder of the SinDDM is frozen and its decoder is fine-tuned through prompt’s guidance. The ROI prompt is added to the original image to mask the areas that do not need editing, while the text prompts would be augmented with PE. Then, we use the frozen image encoder and text encoder of the CLIP to generate corresponding embeddings of the edited image and text prompt, respectively. Finally, we use cosine similarity loss between the two above embeddings as the optimization objective to fine tune the decoder of the SinDDM.



Fig. 8. The generated images with different text prompts. When the prompt is "Large Fire", the edited image area will have an unreasonable result of grass on the deck. However, when the prompt is "heavily burning", the results will much more logical.

burning". You only need to provide the generated text prompt, you do not need to explain why."

Through the above instructions, we can use ChatGPT to generate numerous augmented text, for the text prompt "A ship is on fire", the augmented texts could be "A ship is burning", "A ship is on fire with smokes", "A raging fire on the board" and so on. After that, we obtain the embeddings of the prompts separately from the text encoder of CLIP, and average them as the guidance of the image editing model.

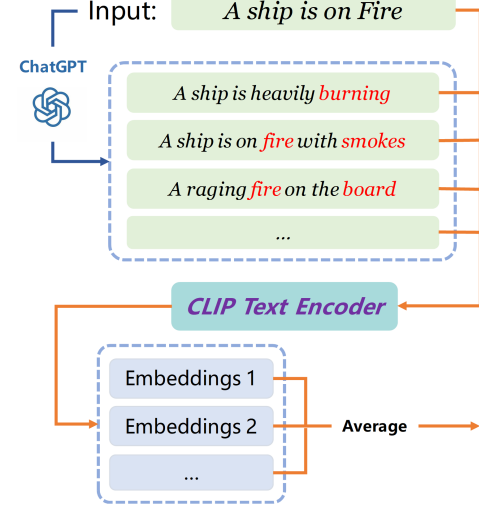


Fig. 9. The overall structure of PE. The text prompt provided by the user is converted into a set of various synonymous texts via GPT, and then the text set is embedded and averaged by the CLIP text encoder as a guide for image editing.

IV. EXPERIMENTS

We evaluate our text-guided RSI editing model through two editing scenarios. First, when comes to the scenario where the type of ground objects is homogeneous and the overall editing is required, we adopt the method of directly repainting the whole image through text guidance to edit the image. Secondly, in the scenario where the types of ground objects are complex and the editing of local areas needs to be refined, we edit it by combining the text guidance and ROI region mask. For the above two scenarios, we take two kinds of datasets:

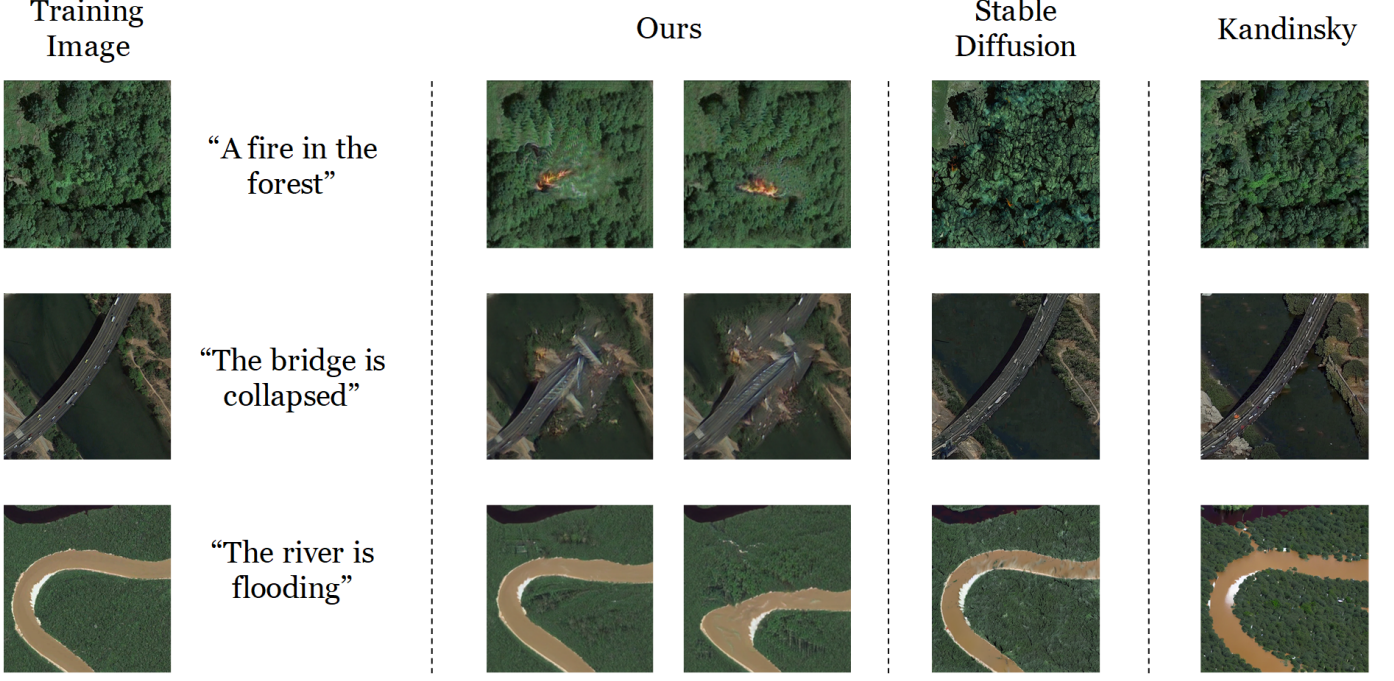


Fig. 10. Generated images of the our proposed method, the Stable Diffusion and the Kandinsky under three scenarios. The above images show the results of full image editing under three scenarios: “A fire in the forest”, “The bridge is collapsed” and “The river is flooding”.

AID [52] and HRSC2016-MS [53].

For the selection of VLMs, in order to introduce the semantic information of RSIs, we use the RemoteCLIP model [54], which is fine-tuned on remote sensing big data. To validate the quality of the edited images quantificationally, we also use CLIP score [55] and a subjective evaluation metric to compare the generation results between our image editing method and mainstream image editing methods such as Stable Diffusion [56] and Kandinsky [57]. CLIP score is calculated by using the CLIP encoder to acquire the features of the edited image and text prompts respectively and computing their cosine similarity.

For the subjective score, we made a suitable questionnaire, using image fidelity and edited quality as the evaluation focus, and asked the experts to give a score from 1 to 5 for each image in the above two aspects. Then, we calculate the comprehensive subjective score by averaging the scores. When conducting a survey, we provide the original image, the requirements for image editing, and the generated images that been edited by different methods, where the edited images are randomly scrambled and not ordered according to the methods. For each edited image, the question we asked the respondents was:

“Please give the scores of the fidelity and the degree of the satisfaction of the needs according to the original image provided and the corresponding editing requirements. The scores are integers from 1 to 5.”

We collected a total of about 200 survey results, about 40% of the interviewee are professional RSI interpreters, about 60% are outside the field of respondents, the knowledge of RSIs is limited to a preliminary understanding. Therefore, the obtained questionnaire can not only assess the satisfaction of the editing

needs with the help of the professional knowledge of remote sensing interpreters, but also evaluate the degree of its fidelity with a large number of non-professionals.

First of all, we test the full image editing performance of each model. There are three scenarios: “A fire in the forest”, “The bridge is collapsed” and “The river is flooding”. The generated images are depicted in the Fig. 10. Intuitively, our generation model is much more complete with the details of the original image beyond the obvious editorial content. When asked to generate a forest on fire, the image produced by our model had a clear flame present, while other models could not. The same goes for the editorial content of the “collapsed bridge”, it can be seen that the images generated by ours faithfully recreate the collapse scene while others just distort the bridge in the image. As to the flooding river, in the images we generated, the river channel is not only biased but also has an impact on the surrounding forest, which is in good agreement with the actual situation.

Different from full image editing, local image editing guided by mask is often more concerned with the degree of refinement and the fusion of mask edges with the original image. To do this, we design three scenarios of image editing tasks focusing on the targets: “The house is damaged”, “Cracks on the storage” and “Big holes on deck”. The generated images are depicted in the Fig.11. Compared to other editing methods, our proposed method also achieved the best results. When generate the image of storage with cracks, our method produces more realistic cracks, which can even simulate shadows and rust caused by the cracks. When generate the damaged house, our proposed method better preserves the outline of the target house, while stable diffusion and Kandinsky significantly change the style of target house. Similarly, when generating

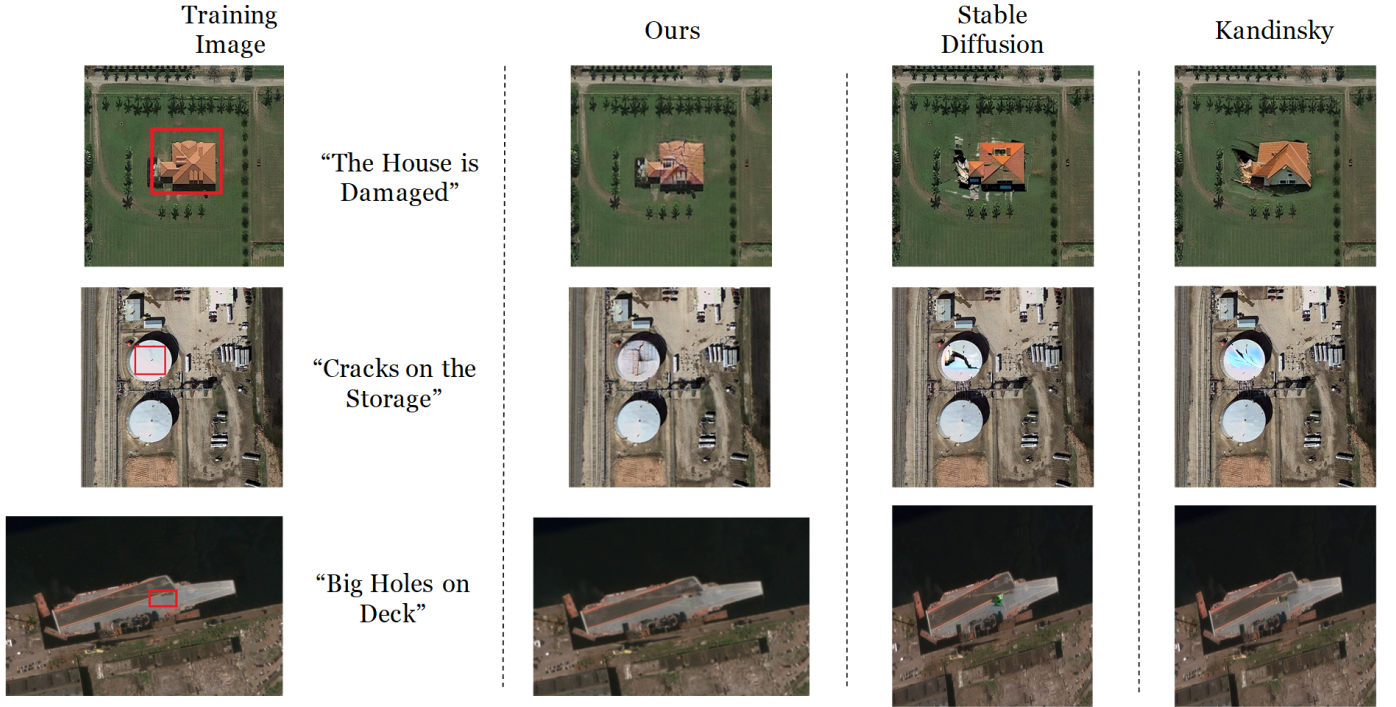


Fig. 11. Generated images of the our proposed method, the Stable Diffusion and the Kandinsky under three scenarios. The above images show the results of local image editing under different scenarios based on the masks: “The house is damaged”, “Cracks on the storage” and “Big holes on deck”.

ship with holes on deck, our results are also more in line with human visual habits.

In contrast, the images generated by Stable Diffusion and Kandinsky display a pronounced phenomenon of semantic confusion and inconsistency. For example, when large cracks are introduced to storage tanks, all generated images—except those produced by our proposed method—exhibit unreasonable colorations. Furthermore, when generating an image of a damaged house, Kandinsky presents an edited depiction from a non-remote sensing perspective. Similarly, when creating large holes on a deck, both aforementioned methods produce irrelevant content in their outputs. These generative flaws can be attributed to several primary factors mentioned in this paper. Firstly, conventional models are trained on large benchmark datasets of natural images, which exhibit significant domain discrepancies compared to remote sensing images. Consequently, these generative models with low generalization struggle to preserve consistency in content and details between the original and edited images, leading to illogical outcomes during image generation. Additionally, these models have been predominantly pre-trained on street-view imagery, resulting in a significant semantic gap between them and the bird’s-eye view RSIs targeted for editing. Lastly, semantic mismatches between textual descriptions and visual representations further exacerbate the confusion observed in the editing results. In contrast to these approaches, our proposed method utilizes a multi-scale training strategy that employs only a single image (the one designated for editing) during DDPM training. Moreover, we leverage RemoteCLIP pre-trained on RSIs to effectively incorporate bird’s-eye view semantic information. Furthermore, PE is employed to alleviate the semantic mis-

match between text and image embeddings, thereby aligning text embeddings more closely with the actual image embeddings. As a result, our proposed method demonstrates superior performance.

TABLE I
QUANTITATIVE EVALUATION RESULTS OF COMPARATIVE METHODS. THE HIGHEST SCORE IS HIGHLIGHTED IN BOLD.

		Ours	Stable Diffusion	Kandinsky
CLIP Score	Forest	21.38	19.94	17.24
	Bridge	22.64	21.08	21.26
	River	20.11	19.38	19.16
	House	22.76	21.98	21.55
	Storage	17.98	15.48	15.94
	Ship	14.68	10.83	11.55
Subjective Score	Forest	4.50	4.15	3.76
	Bridge	4.56	4.03	4.11
	River	4.25	3.93	4.41
	House	4.65	4.25	4.13
	Storage	4.59	4.27	4.06
	Ship	4.44	3.94	4.23

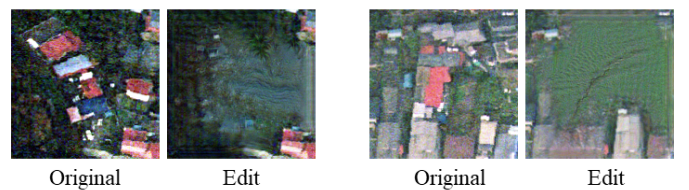


Fig. 12. RSIs of buildings before the tsunami and corresponding post-tsunami images generated in prompt “a picture of ground after tsunami”. Here are some examples.

The Table I shows the quantitative evaluation metrics

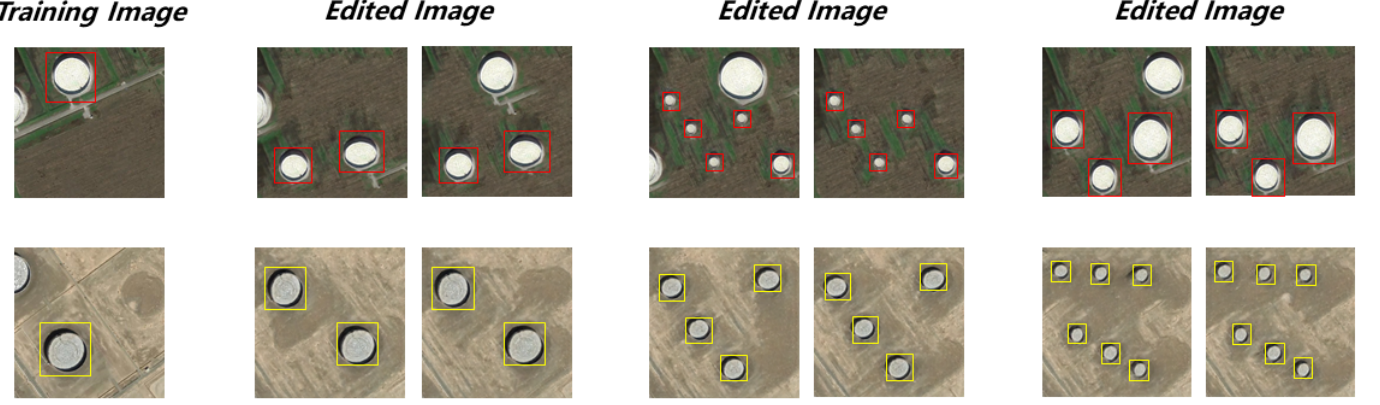


Fig. 13. The edited images of the oil storage tanks via the ROI-prompted image editing method.

of edited images generated by different models under the various scenarios. Firstly, as to the CLIP score, our proposed model achieves optimal results in all scenarios. This shows that the images generated by our model are more consistent with the content of the edited text. In addition to objective evaluation metrics, subjective evaluation is equally important for evaluating image quality. After expert testing, the image generated by our proposed model achieved the highest scores in most scenarios, which shows that they're more consistent with human vision and more logical. What we have to admit is that due to length limitations, more experimental results will not be presented in the paper, but they are available at https://github.com/HIT-PhilipHan/remote_sensing_image_editing.

TABLE II
THE EXPERIMENTAL RESULTS OF BUILDING DAMAGE ESTIMATION WITH
DIFFERENT TRAINING SET.

	5 pairs	10 pairs	30 pairs	50 pairs
Only Observed Samples	68.74	71.82	81.66	89.42
With Generated Samples	70.92	73.39	85.14	91.07

To validate the proposed image editing method for supporting remote sensing tasks, we used the disaster change detection and assessment dataset [58], generating post-disaster images with the prompt “a picture of ground after tsunami” to construct the training dataset, some samples are shown in Fig. 12. Using a Siamese network based on ResNet18, we input pre- and post-disaster images to estimate building destruction. We combined generated data pairs with real observation data pairs and compared test set accuracy. Each experiment included 30 pairs of undamaged house images additionally. The results, shown in Table II, demonstrate that our generated post-disaster images effectively supplement real observation images. When the experiment is set to 5 pairs, 10 pairs, 30 pairs and 50 pairs, the prediction accuracy of the model after adding the generated image pairs is higher than that using only the observation data, and the accuracy improvement is 2.45%, 1.57%, 3.48% and 1.65% respectively.

In addition to augmenting datasets for disaster change detection tasks, our proposed image editing method can be effectively utilized in areas such as urban planning and critical

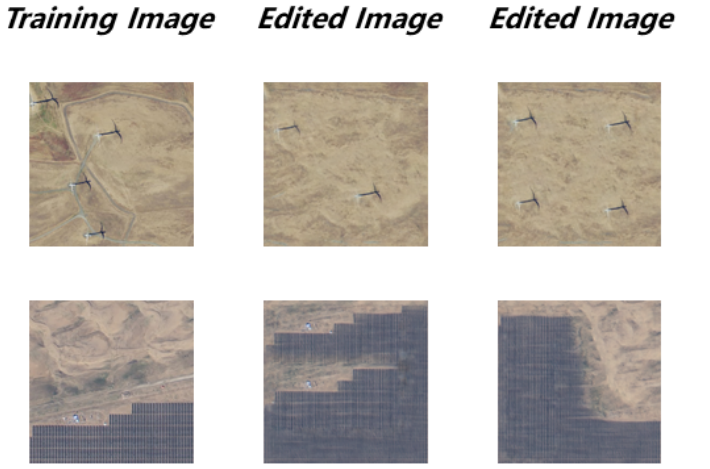


Fig. 14. More applications of the image editing method, for example, generating photovoltaic panels, wind turbine and so on at specified locations in the RSIs.

target detection. For instance, oil storage tanks play a vital role in the global economy, yet information about oil production, consumption, and storage is often concealed for economic or military reasons. Thus, analyzing and processing satellite images combined with deep learning algorithms is a key approach to rapidly monitor the number of oil tanks in a given region. Our image editing method can significantly aid in oil tank detection by generating RSIs that feature oil tanks within diverse geographic backgrounds. Furthermore, it enables the creation of comparative image pairs before and after oil tank construction, supporting tasks like change detection. In our experiment, we employ ROI-prompted image editing to generate RSIs containing oil tanks in various backgrounds, while also controlling the size and number of oil storage tanks in the edited images. The results are presented in Fig. 13.

The experimental results indicate that our method can not only generate oil tanks of varying sizes and quantities in designated areas but also ensure effective integration of the oil tanks with their respective image backgrounds, maintaining consistency in content and details. In addition to generating RSIs featuring oil tanks, our proposed method is capable of producing photovoltaic panels and wind turbines at specified

locations, thereby facilitating tasks in specific remote sensing domains. We will present several results generated using the ROI prompt, including site-specific photovoltaic panels and wind turbines. The results are illustrated in Fig. 14.

In Fig. 14, the generated RSIs of photovoltaic panels, wind turbine possess high image fidelity, which can alleviate the acquirement for a lot of demand of remote sensing data in specific fields. However, we have to admit that our method is still lacking in the reproduction of high frequency information such as image details and edges, so the generated RSIs containing photovoltaic panels panels are fuzzy inevitably, which should be paid more attention to in the subsequent work.

V. CONCLUSIONS

In this paper, we first address the issue of RSIs editing, a topic that has been relatively overlooked in remote sensing research. We then propose a novel method to achieve stable and controllable prompt-guided RSI editing, utilizing only a single image for training. By employing a multi-scale training strategy and conducting DDPM training with just one sample, we preserve consistency in content and details between the original and edited images and mitigate the challenges associated with scarce training data. Additionally, we leverage VLMs pre-trained on RSI datasets to integrate remote sensing information into the image editing process, using PE to alleviate semantic mismatches between text and image embeddings. Alongside satisfactory visual results, our quantitative evaluation metrics, including CLIP scores and subjective assessments, demonstrate that our method outperforms existing image editing models for RSIs. Furthermore, we apply the generated edited images to support disaster assessment efforts, specifically to evaluate whether a building was destroyed by a tsunami, yielding satisfactory experimental outcomes. In future work, we aim to further minimize the loss of high-frequency information during image editing while ensuring the completion of editing tasks, enhancing the preservation of edge outlines and delineations of small targets, and expanding the applicability of image editing techniques.

REFERENCES

- [1] X. Xing, B. Yu, C. Kang, B. Huang, J. Gong, and Y. Liu, “The synergy between remote sensing and social sensing in urban studies: Review and perspectives,” *IEEE Geosci. Remote Sens. Mag.*, vol. 12, no. 1, pp. 108–137, 2024.
- [2] K. Chen, B. Chen, C. Liu, W. Li, Z. Zou, and Z. Shi, “Rsmamba: Remote sensing image classification with state space model,” *IEEE Geosci. Remote Sens. Lett.*, vol. 21, pp. 1–5, 2024.
- [3] J. Klys, J. Snell, and R. Zemel, “Learning latent subspaces in variational autoencoders,” in *Proc. Adv. Neural Inf. Process. Syst.*, vol. 31, pp. 6444–6454, 2018.
- [4] T. Zhou, Q. Li, H. Lu, Q. Cheng, and X. Zhang, “Gan review: Models and medical image fusion applications,” *Inf. Fusion*, vol. 91, pp. 134–148, 2023.
- [5] J. Gu, Y. Shen, and B. Zhou, “Image processing using multi-code gan prior,” in *Proc. IEEE Conf. Comput. Vis. Pattern Recognit.*, pp. 3012–3021, 2020.
- [6] X. Pan, J. Zhao, and J. Xu, “Conditional generative adversarial network-based training sample set improvement model for the semantic segmentation of high-resolution remote sensing images,” *IEEE Trans. Geosci. Remote Sens.*, vol. 59, no. 9, pp. 7854–7870, 2021.
- [7] R. Zhang, Z. Cao, S. Yang, L. Si, H. Sun, L. Xu, and F. Sun, “Cognition-driven structural prior for instance-dependent label transition matrix estimation,” *IEEE Trans. Neural Netw. Learn. Syst.*, pp. 1–14, 2024.
- [8] Y. Cui, P. Liu, B. Song, L. Zhao, Y. Ma, and L. Chen, “Reconstruction of large-scale missing data in remote sensing images using extend-gan,” *IEEE Geosci. Remote Sens. Lett.*, vol. 21, pp. 1–5, 2024.
- [9] K. Jiang, Z. Wang, P. Yi, G. Wang, T. Lu, and J. Jiang, “Edge-enhanced gan for remote sensing image superresolution,” *IEEE Trans. Geosci. Remote Sens.*, vol. 57, no. 8, pp. 5799–5812, 2019.
- [10] H. Li, W. Deng, Q. Zhu, Q. Guan, and J. Luo, “Local-global context-aware generative dual-region adversarial networks for remote sensing scene image super-resolution,” *IEEE Trans. Geosci. Remote Sens.*, vol. 62, pp. 1–14, 2024.
- [11] C. Wang, X. Zhang, W. Yang, G. Wang, X. Li, J. Wang, and B. Lu, “Msawgan: Multispectral remote sensing image super-resolution based on multiscale window attention transformer,” *IEEE Trans. Geosci. Remote Sens.*, vol. 62, pp. 1–15, 2024.
- [12] K. Doi, K. Sakurada, M. Onishi, and A. Iwasaki, “Gan-based sar-to-optical image translation with region information,” in *Proc. IEEE Int. Geosci. Remote Sens. Symp.*, pp. 2069–2072, 2020.
- [13] R. Zhang, L. Li, Q. Zhang, J. Zhang, L. Xu, B. Zhang, and B. Wang, “Differential feature awareness network within antagonistic learning for infrared-visible object detection,” *IEEE Trans. Circuits Syst. Video Technol.*, pp. 1–1, 2023.
- [14] Z. Guo, Z. Zhang, Q. Cai, J. Liu, Y. Fan, and S. Mei, “Ms-gan: Learn to memorize scene for unpaired sar-to-optical image translation,” *IEEE J. Sel. Topics Appl. Earth Observ. Remote Sens.*, vol. 17, pp. 11467–11484, 2024.
- [15] Y. Zhao, S. Shen, J. Hu, Y. Li, and J. Pan, “Cloud removal using multimodal gan with adversarial consistency loss,” *IEEE Geosci. Remote Sens. Lett.*, vol. 19, pp. 1–5, 2022.
- [16] J. Li, Z. Wu, Z. Hu, J. Zhang, M. Li, L. Mo, and M. Molinier, “Thin cloud removal in optical remote sensing images based on generative adversarial networks and physical model of cloud distortion,” *ISPRS J. Photogramm. Remote Sens.*, vol. 166, pp. 373–389, 2020.
- [17] J. Zhang, J. Huang, S. Jin, and S. Lu, “Vision-language models for vision tasks: A survey,” *IEEE Trans. Pattern Anal. Mach. Intell.*, vol. 46, no. 8, pp. 5625–5644, 2024.
- [18] A. Radford, J. W. Kim, C. Hallacy, A. Ramesh, G. Goh, S. Agarwal, G. Sastry, A. Askell, P. Mishkin, J. Clark, G. Krueger, and I. Sutskever, “Learning transferable visual models from natural language supervision,” *arXiv preprint arXiv:2103.00020*, 2021.
- [19] J. Ho, A. Jain, and P. Abbeel, “Denoising diffusion probabilistic models,” *arXiv preprint arXiv:2006.11239*, 2020.
- [20] W. Xia, Y. Yang, J.-H. Xue, and B. Wu, “Tedigan: Text-guided diverse face image generation and manipulation,” in *Proc. IEEE Conf. Comput. Vis. Pattern Recognit.*, pp. 2256–2265, 2021.
- [21] O. Patashnik, Z. Wu, E. Shechtman, D. Cohen-Or, and D. Lischinski, “Styleclip: Text-driven manipulation of stylegan imagery,” in *Proc. IEEE Int. Conf. Comput. Vis.*, pp. 2085–2094, 2021.
- [22] Y. Huang, J. Huang, Y. Liu, M. Yan, J. Lv, J. Liu, W. Xiong, H. Zhang, S. Chen, and L. Cao, “Diffusion model-based image editing: A survey,” *arXiv preprint arXiv:2402.17525*, 2024.
- [23] N. Huang, Y. Zhang, F. Tang, C. Ma, H. Huang, W. Dong, and C. Xu, “Diffstyler: Controllable dual diffusion for text-driven image stylization,” *IEEE Trans. Neural Networks Learn. Syst.*, pp. 1–14, 2024.
- [24] Z. Wang, L. Zhao, and W. Xing, “Stylediffusion: Controllable disentangled style transfer via diffusion models,” in *Proc. IEEE Int. Conf. Comput. Vis.*, pp. 7677–7689, October 2023.
- [25] R. Mokady, A. Hertz, K. Aberman, Y. Pritch, and D. Cohen-Or, “Null-text inversion for editing real images using guided diffusion models,” in *Proc. IEEE Conf. Comput. Vis. Pattern Recog.*, pp. 6038–6047, June 2023.
- [26] Y. Zhang, N. Huang, F. Tang, H. Huang, C. Ma, W. Dong, and C. Xu, “Inversion-based style transfer with diffusion models,” in *Proc. IEEE Conf. Comput. Vis. Pattern Recog.*, pp. 10146–10156, June 2023.
- [27] B. Wallace, A. Gokul, and N. Naik, “Edict: Exact diffusion inversion via coupled transformations,” in *Proc. IEEE Conf. Comput. Vis. Pattern Recog.*, pp. 22532–22541, June 2023.
- [28] D. Epstein, A. Jabri, B. Poole, A. Efros, and A. Holynski, “Diffusion self-guidance for controllable image generation,” in *Proc. Adv. Neural Inf. Process. Syst.*, vol. 36, pp. 16222–16239, 2023.
- [29] B. Kawar, S. Zada, O. Lang, O. Tov, H. Chang, T. Dekel, I. Mosseri, and M. Irani, “Imagic: Text-based real image editing with diffusion models,” in *Proc. IEEE Conf. Comput. Vis. Pattern Recog.*, pp. 6007–6017, June 2023.
- [30] P. Ghamisi, B. Rasti, N. Yokoya, Q. Wang, B. Hofle, L. Bruzzone, F. Bovolo, M. Chi, K. Anders, R. Gloaguen, P. M. Atkinson, and J. A. Benediktsson, “Multisource and multitemporal data fusion in remote

sensing: A comprehensive review of the state of the art,” *IEEE Geosci. Remote Sens. Mag.*, vol. 7, no. 1, pp. 6–39, 2019.

[31] Z. Li, F. Lu, J. Zou, L. Hu, and H. Zhang, “Generalized few-shot meets remote sensing: Discovering novel classes in land cover mapping via hybrid semantic segmentation framework,” in *Proc. IEEE Conf. Comput. Vis. Pattern Recog.*, pp. 2744–2754, June 2024.

[32] L. Ma, X. Wang, and L. Du, “YJWS2023: high-resolution optical remote sensing image dataset of typical military ship target,” in *Sixth Conference on Frontiers in Optical Imaging and Technology: Imaging Detection and Target Recognition*, vol. 13156, p. 131560L, 2024.

[33] L. Si, H. Dong, W. Qiang, Z. Song, B. Du, J. Yu, and F. Sun, “A trusted generative-discriminative joint feature learning framework for remote sensing image classification,” *IEEE Trans. Geosci. Remote Sens.*, vol. 62, p. 5601814, 2024.

[34] L. Zhang and Y. Liu, “Remote sensing image generation based on attention mechanism and vae-msgan for roi extraction,” *IEEE Geosci. Remote Sens. Lett.*, vol. 19, pp. 1–5, 2022.

[35] H. Chen, W. Li, and Z. Shi, “Adversarial instance augmentation for building change detection in remote sensing images,” *IEEE Trans. Geosci. Remote Sens.*, vol. 60, pp. 1–16, 2022.

[36] R. Dong, L. Zhang, and H. Fu, “Rrsgan: Reference-based super-resolution for remote sensing image,” *IEEE Trans. Geosci. Remote Sens.*, vol. 60, pp. 1–17, 2022.

[37] B. Song, P. Liu, J. Li, L. Wang, L. Zhang, G. He, L. Chen, and J. Liu, “Mlff-gan: A multilevel feature fusion with gan for spatiotemporal remote sensing images,” *IEEE Trans. Geosci. Remote Sens.*, vol. 60, pp. 1–16, 2022.

[38] X. Yang, Z. Wang, J. Zhao, and D. Yang, “Fg-gan: A fine-grained generative adversarial network for unsupervised sar-to-optical image translation,” *IEEE Trans. Geosci. Remote Sens.*, vol. 60, pp. 1–11, 2022.

[39] Y. Xiao, Q. Yuan, K. Jiang, J. He, X. Jin, and L. Zhang, “Ediffrs: An efficient diffusion probabilistic model for remote sensing image super-resolution,” *IEEE Trans. Geosci. Remote Sens.*, vol. 62, pp. 1–14, 2024.

[40] Y. Zhang, H. Liu, Z. Li, X. Gao, G. Shi, and J. Jiang, “Tcdm: Effective large-factor image super-resolution via texture consistency diffusion,” *IEEE Trans. Geosci. Remote Sens.*, vol. 62, pp. 1–13, 2024.

[41] W. Peebles and S. Xie, “Scalable diffusion models with transformers” in *Proc. IEEE Int. Conf. Comput. Vis.*, pp. 4195–4205, October 2023.

[42] D. Kingma, T. Salimans, B. Poole, and J. Ho, “Variational diffusion models,” in *Proc. Adv. Neural Inf. Process. Syst.*, vol. 34, pp. 21696–21707, 2021.

[43] J. Ho, T. Salimans, A. Gritsenko, W. Chan, M. Norouzi, and D. J. Fleet, “Video diffusion models,” in *Proc. Adv. Neural Inf. Process. Syst.*, vol. 35, pp. 8633–8646, 2022.

[44] J. Wu, R. FU, H. Fang, Y. Zhang, Y. Yang, H. Xiong, H. Liu, and Y. Xu, “Medsegdiff: Medical image segmentation with diffusion probabilistic model,” in *Medical Imaging with Deep Learning*, vol. 227, pp. 1623–1639, 2024.

[45] R. Yang and S. Mandt, “Lossy image compression with conditional diffusion models,” in *Proc. Adv. Neural Inf. Process. Syst.*, vol. 36, pp. 64971–64995, 2023.

[46] M. Kwon, J. Jeong, and Y. Uh, “Diffusion models already have a semantic latent space,” *arXiv preprint: arXiv 2210.10960*, 2023.

[47] Z. Pan, R. Gherardi, X. Xie, and S. Huang, “Effective real image editing with accelerated iterative diffusion inversion,” in *Proc. IEEE Int. Conf. Comput. Vis.*, pp. 15912–15921, October 2023.

[48] K. Han, Y. Wang, H. Chen, X. Chen, J. Guo, Z. Liu, Y. Tang, A. Xiao, C. Xu, Y. Xu, Z. Yang, Y. Zhang, and D. Tao, “A survey on vision transformer,” *IEEE Trans. Pattern Anal. Mach. Intell.*, vol. 45, no. 1, pp. 87–110, 2023.

[49] M. U. Khattak, H. Rasheed, M. Maaz, S. Khan, and F. S. Khan, “Maple: Multi-modal prompt learning,” in *Proc. IEEE Conf. Comput. Vis. Pattern Recog.*, pp. 19113–19122, June 2023.

[50] Y. Liu, Y. Lu, H. Liu, Y. An, Z. Xu, Z. Yao, B. Zhang, Z. Xiong, and C. Gui, “Hierarchical prompt learning for multi-task learning,” in *Proc. IEEE Conf. Comput. Vis. Pattern Recog.*, pp. 10888–10898, June 2023.

[51] J. Park, J. Ko, and H. J. Kim, “Prompt learning via meta-regularization,” in *Proc. IEEE Conf. Comput. Vis. Pattern Recog.*, pp. 26940–26950, June 2024.

[52] G.-S. Xia, J. Hu, F. Hu, B. Shi, X. Bai, Y. Zhong, L. Zhang, and X. Lu, “Aid: A benchmark data set for performance evaluation of aerial scene classification,” *IEEE Trans. Geosci. Remote Sens.*, vol. 55, no. 7, pp. 3965–3981, 2017.

[53] W. Chen, B. Han, Z. Yang, and X. Gao, “Mssdet: Multi-scale ship-detection framework in optical remote-sensing images and new benchmark,” *Remote Sens.*, vol. 14, no. 21, p. 5460, 2022.

[54] F. Liu, D. Chen, Z. Guan, X. Zhou, J. Zhu, Q. Ye, L. Fu, and J. Zhou, “Remoteclip: A vision language foundation model for remote sensing,” *arXiv preprint: arXiv 2306.11029*, 2023.

[55] J. Hessel, A. Holtzman, M. Forbes, R. L. Bras, and Y. Choi, “Clipscore: A reference-free evaluation metric for image captioning,” *arXiv preprint: arXiv 2104.08718*, 2021.

[56] R. Rombach, A. Blattmann, D. Lorenz, P. Esser, and B. Ommer, “High-resolution image synthesis with latent diffusion models,” 2021.

[57] A. Shakhmatov, A. Razzhigaev, A. Nikolich, V. Arkhipkin, I. Pavlov, A. Kuznetsov, and D. Dimitrov, “Kandinsky 2.1,” 2023.

[58] A. Fujita, K. Sakurada, T. Imaizumi, R. Ito, S. Hikosaka, and R. Nakamura, “Damage detection from aerial images via convolutional neural networks,” in *Proc. IAPR Int. Conf. Mach. Vis. Appl.*, pp. 5–8, 2017.



Fangzhou Han received the B.E. degree in information and communication engineering from Harbin Institute of Technology, Harbin, China. He is currently pursuing the M.S. degree with Harbin Institute of Technology, Harbin, China. His research interests include deep learning, SAR image processing and causal inference.



Lingyu Si received the M.S. degree from University of Bristol, in 2018, and the Ph.D. degree from University of Chinese Academy of Sciences, Beijing, China, in 2024. His research interests include transfer learning and self-supervised learning.



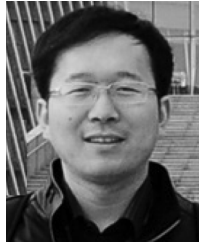
Hongwei Dong (Member, IEEE) received the M.S. degree from China Agricultural University, Beijing, China, in 2018, and the Ph.D. degree from Harbin Institute of Technology, Harbin, China, in 2022. He is currently a associate research fellow with the Department of Information Engineering, Harbin Institute of Technology. His current research interests include applied mathematics, optimization methods, and machine learning.



Lamei Zhang (Senior Member, IEEE) received the B.S., M.Sc., and Ph.D. degrees in information and communication engineering from Harbin Institute of Technology, Harbin, China, in 2004, 2006, and 2010, respectively. She is currently an Associate Professor with the Department of Information Engineering, Harbin Institute of Technology. Her research interests include RSIs processing, information extraction and interpretation of high-resolution synthetic aperture radar, polarimetric SAR, and polarimetric SAR interferometry. Dr. Zhang serves as the Secretary for the IEEE Harbin Education Section.



Hao Chen (Member, IEEE) received the B.S., M.S., and Ph.D. degrees from Harbin Institute of Technology, Harbin, China, in 2001, 2003, and 2008, respectively. Since 2004, he has been with the School of Electronics and Information Engineering, Harbin Institute of Technology. He is currently a Professor. His main research interests include RSI processing and image compression.



Bo Du (Senior Member, IEEE) received the B.S. degree and the Ph.D. degree in photogrammetry and remote sensing from the State Key Laboratory of Information Engineering in Surveying, Mapping and Remote Sensing, Wuhan University, Wuhan, China, in 2005, and in 2010, respectively. He is currently a Professor with the School of Computer Science and Institute of Artificial Intelligence, Wuhan University, where he is also the Director of the National Engineering Research Center for Multimedia Software. He has more than 80 research articles published in IEEE Transactions on Image Processing, IEEE Transactions on Cybernetics, IEEE Transactions on Pattern Analysis and Machine Intelligence, and IEEE Transactions on Geoscience and Remote Sensing; 14 of them are ESI hot papers or highly cited papers. His major research interests include machine learning, computer vision, and image processing.